EFFECTS OF SCANDIUM ON RAPID SOLIDIFIED HYPO-EUTECTIC ALUMINUM COPPER

A-A. Bogno[1], H. Henein[1], D.G. Ivey[1], J. Valloton[1], G. Reinhart[2], D. Sediako[3], M. Gallerneault[4],

[1]Department of Chemical and Materials Engineering, University of Alberta
Edmonton, Alberta, Canada T6G 1H9

[2]Aix-Marseille University and CNRS, IM2NP UMR 7334, Campus Saint-Jérôme, Case 142, 13397 Marseille Cedex 20, France

[3]School of Engineering, University of British Colombia, Okanagan Campus
Kelowna, BC, Canada V1V 1V7

[4]Alcereco Inc. Kingston, Ontario, Canada K7L 3N6

Abstract

This paper reports on the characterization of rapidly solidified Al-4.5 wt% Cu-xSc (x= 0.1, 0.2 or 0.4 wt %). The effect of micro-additions of Sc (up to 0.4 wt %) was examined through microstructural analysis of rapidly solidified, as well as aged samples, by means of electron microscopy, x-ray and neutron diffraction and microhardness measurements. The effect of micro-additions of Sc on the scale of the rapid solidified microstructure was negligible. The Sc additions were supersaturated mainly in the interdendritic regions. However, upon aging of the samples, directly after rapid solidification, nano-precipitates rich in Sc were observed in the matrix and some Sc was also associated with the θ phase. No W phase was observed in either as atomized or aged samples. Furthermore, dramatic improvements in mechanical properties (specifically hardness) were achieved. This work highlights the use of various and complementary tools to characterize the effect of micro-additions of Sc to hypoeutectic Al-Cu alloys over a wide range of solidification thermal histories. It also demonstrates the capability of designing alloys and process strategies with unique microstructures and mechanical properties superior to age hardened Al-4.5 wt% Cu alloys.

1.   Introduction

The choice of Al alloys for industrial products is generally justified by their density, good mechanical performance, corrosion resistance and castability [1]. Although Al-Si is the most widely used Al alloy in the automotive industry [2], high efficiency car engines require alloys such as Al-Cu, with higher service temperatures than Al-Si [3,4]. Indeed, from a mechanical properties point of view, Al-Cu alloys are potential alternatives to Al-Si as they present better mechanical performance at temperatures higher than 250°C [5]. The microstructure of as-cast Al-Cu alloys consists of an age hardenable α-Al matrix and various types of aluminides (depending on the alloy composition) in the inter-cellular regions. Al-Cu alloys are, therefore, the first choice for strength requirements [6].

The classical approach for strengthening age hardenable Al-Cu alloys consists of casting the alloy, followed by heat treatment. Heat treatment usually involves solutionizing the alloy in order to dissolve all Cu-bearing precipitates, followed by quenching and age hardening. This route promotes the formation of highly dispersed precipitates in the matrix [7].

The addition of Sc to Al-Cu alloys is reported to promote not only age hardening through the precipitation of finely dispersed Al_3Sc particles that can tightly pin the grain boundaries and dislocations, but also effective grain refining [8]. Industrial applications of Sc containing Al-alloys includes automotive, avionic, sports equipment, etc. However, Sc is an expensive alloying addition, when compared with industrially established Ti/B grain refiners and its solubility in Al at room temperature is very low (maximum solubility is 0.38 wt% at 659°C). In addition, the solubility of Cu in Al decreases with increasing Sc and Sc promotes the formation of $Al_{8-x}Cu_{4+x}Sc$, the so-called W-phase, which has a detrimental effect on the mechanical properties of the alloy product [7]. It is, therefore, desirable to use a minimal Sc addition for maximum benefit to the final product.

At low solidification rates (0.01, 0.08, 0.3 and 0.8°C s^{-1}), it was shown in a separate study [9] that the addition of Sc to Al-4.5 wt% Cu leads to the formation of the insoluble W-phase, resulting in the consumption of Sc and Cu. This negatively affected the precipitation of Al_3Sc and Al_2Cu strengthening phases.

It is expected that at high solidification rates, the solid solubility of Sc in Al will be extended. A metastable supersaturated solid solution would result in an increased amount of the Al_3Sc strengthening phase on subsequent heat treatment (aging) in the temperature range of 250°C to

350°C [8]. In addition, formation of the W-phase can be minimized. The metastable extension of the solubility of Sc in Al can be achieved by promoting a large amount of nucleation undercooling, which occurs during rapid solidification of the alloy.

[Figure 1 near here]

It has been previously shown that a large amount of nucleation undercooling induces extension of the solidus and liquidus lines. The result of these extensions, as predicted by Thermo-Calc [10, 11] and shown in Figure 1, is the supersaturation of Cu and Sc in the α-Al matrix so that upon aging, precipitation of fine Al_2Cu and Al_3Sc particles may be fostered.

In 1960, Pol Duwez discovered that metastable effects resulting from very high cooling rates were achieved during the solidification of droplets impacting a chilled substrate. These effects included retention of a single phase with an fcc structure in an Ag–Cu alloy [12], rather than two phases as predicted under equilibrium conditions. The formation of a metallic glass was reported in an Au–Si system [13]. Based on these discoveries, various improvements to Duwez's melt quenching technique were introduced; these include splat-quenching [14–16], melt-spinning [17–19], atomization [20–27] and levitation [28–31].

In this work, impulse atomization (IA) [25], a containerless solidification technique, was used to generate rapidly solidified Al-4.5 wt% Cu-xSc (x= 0.1, 0.2 or 0.4 wt %) samples. IA offers a unique opportunity to achieve far-from-equilibrium microstructures through high cooling rates and large undercooling. IA has the ability to generate several droplets during a single experimental run, with tailored microstructures due to the inherent differences in cooling rate determined by droplet size, atmosphere and superheating [32–34]. This paper studies the effects of Sc additions at hypoeutectic levels (0.1 wt%, 0.2 wt% and 0.4 wt%) on the microstructure (cell spacing) and mechanical properties (hardness) of rapidly solidified Al-4.5 wt% Cu droplets, before and after heat treatment.

2. Materials and methods

2.1. Sample production

Rapid solidification of Al-4.5 wt% xSc (x= 0.1, 0.2 and 0.4 wt% Sc) alloys was achieved by IA. A detailed description of the technique is given elsewhere. To obtain the investigated IA samples, 350 g of each pre-alloyed composition were melted in a dense, high purity, graphite crucible (grade: GR001CC) using a high frequency induction furnace. Prior to atomization, each alloy was

heated to 200°C above its liquidus temperature under an Ar or He atmosphere in an almost oxygen free (10 ppm) atomization chamber. IA droplets with sizes varying from 212 μm to 1000 μm were investigated. A wide range of droplets sizes, generated in a single run by IA, provides various thermal histories to be investigated. However, due to the experimental difficulties in monitoring the temperature history of the droplets in flight during IA, the nucleation temperature and cooling rate of the droplets could not be measured. Consequently, the thermal history of each IA droplet was predicted using a numerical model developed by Wiskel et al [32, 33] and the nucleation undercooling was determined using a methodology developed in [34]. The numerical model is based on the quantification of heat exchange between an IA droplet and the stagnant gas in an environment with a large temperature gradient. Nucleation undercooling determination was based on measurement of the eutectic fraction combined with the coarsening model of secondary dendrite arm spacing.

2.2. Microstructural analysis and mechanical property evaluation

Microstructural analysis was achieved by neutron diffraction (ND), scanning electron microscopy (SEM) and electron micro-probe analysis (EPMA). The mechanical properties were evaluated through Vickers microhardness measurements.

Prior to microstructural characterization and mechanical property evaluation, the investigated samples (in powder form) were mounted in epoxy resin, ground with silicon carbide grinding papers and polished with diamond suspension pastes. The final polish was done with 0.05 μm colloidal silica.

2.2.1. Neutron diffraction (ND)

ND was carried out to identify and quantify the microstructural phases. The experiments were performed on a C2 neutron powder diffractometer equipped with an 800 wire BF3 position sensitive detector that floats on an epoxy resin. The technique consists of directly correlating the normalized intensity of a diffracted monochromatic neutron beam at a specific range of 2 theta angles with the amount of phase that has Bragg peaks within this range of 2 theta angles [35–41]. Encapsulated into cylindrical vanadium cans, the samples were illuminated by a neutron beam through beam-defining slits. A neutron wavelength of 1.33 Å generated from a Si-531 monochromator was used for the measurements. A wide-angle detector was utilized to collect

neutrons at diffraction angles (2 theta) ranging from 30˚ to 110˚, enabling a plot of neutron diffraction intensity as a function of 2 theta. In addition, an experiment with an empty crucible was carried out using the same parameters to establish an accurate background, enabling the subtraction of miscellaneous peaks generated from the interaction of neutrons with surrounding equipment such as the sample holder and impurities in the V crucible used to contain the samples. Rietveld refinement analysis [42] was applied, through Topas software [43], to determine the weight fractions and lattice spacings of the phases in the as-solidified samples.

2.2.2. SEM and EPMA

SEM was used to visualize the microstructures (morphology and length scale) of the investigated samples. The analysis was carried out using a Tescan Vega3 instrument equipped with an energy dispersive X-ray (EDX) analysis system (INCA Microanalysis System, Oxford Instruments). Imaging was done in backscattered electron (BSE) mode (to provide atomic number (Z) contrast), at an accelerating voltage of 10 kV.

EPMA was used for X-ray elemental mapping of Al, Cu and Sc by wavelength dispersive spectroscopy (WDS). The analysis was performed using a JEOL 8900R electron microprobe at an accelerating voltage of 20 kV.

2.2.3. TEM

TEM was used to visualize and identify precipitates that could not be detected by SEM and EPMA analyses. TEM was performed with a JEOL 2010 instrument operated at 200 kV and equipped with an ultra-thin window EDX detector. The TEM specimens were prepared using focused ion beam (FIB) milling with a Hitachi NB 5000 dual-beam FIB/SEM

2.2.4. Cell spacing and hardness evaluation

The microstructural length scale was evaluated by considering the average cell spacing (equal to the average cell size) as visualized in 2D micrographs. The center-to-center distance between two cells was measured by applying the line intercept method according to ASTM E112-13. The mechanical properties were evaluated through microhardness measurements of both the as-solidified and heat treated samples using a Buehler VH3100 microhardness tester, calibrated with a steel block provided by the manufacturer. A minimum of five indentations were randomly applied to each sample with a load of 100 gf for a holding time of 10 s.

2.3. Heat treatment

The typical heat treatment procedure for Al alloys includes the dissolution of all solute elements into the stable α-Al phase (solutionizing). To ensure that the solid solution phase is retained, the sample is quenched to room temperature. After quenching, the solid solution is supersaturated with solute elements (Cu and Sc in this case) and there exists a driving force, induced by aging of the supersaturated solid solution, for precipitation of the equilibrium phases, Al_2Cu and Al_3Sc. The equilibrium θ-Al_2Cu phase is typically preceded by the formation of transition phases, i.e., Guinier-Preston zones (GP-zones), θ''-Al_2Cu and θ'-Al_2Cu [44]; however, to the authors' knowledge, no GP-zones or other transition phases have been reported prior to the formation of Al_3Sc.

In this work, two heat treatment approaches, schematically described in Figure 2, were used on the as-solidified samples. The first heat treatment approach, HT1, had 6 steps. In a carbolite furnace, the samples were solutionized by heating to 535°C (Step 1) and soaking at this temperature for 18.5 h to dissolve secondary precipitates (Step 2). After solutionizing, the samples were quenched in a cold water bath (~10°C) (Step 3). Following quenching, the samples were heated to 240°C (Step 4) and held for 2 h to age (Step 5) before water quenching to room temperature (Step 6). HT1 was meant to replicate typical industrial heat treatment processes in which dissolution of the intermetallics for solute supersaturation in the matrix is followed by aging to induce precipitation hardening (age hardening) [45].

[Figure 2 near here]

The aging temperature range of hypoeutectic Al-Cu alloys is reported to vary from 100°C to 250°C [8] and the aging temperature for hypoeutectic Al-Sc alloys varies from 250°C to 350°C [46]. The maximum strength for Al-Cu of similar composition (4 wt% Cu) is reported to occur upon aging at 240°C for 2 h after solutionizing [47], [48], [49], [49]. The optimum solutionizing temperature and holding time for a hypoeutectic Al-4 wt% Cu, as calculated and reported in [48], are 527°C and 10 h. However, corresponding parameters have not been reported for Al-Cu-Sc. Consequently, due to the low diffusivity of Sc in Al compared with Cu, the solutionizing temperature for Al-4.5 wt% Cu-0.4 wt% Sc, in HT1, was increased to 535°C which is about 10°C lower than the melting

temperature of the eutectic structure. An aging temperature of 240°C and a holding time of 2 h were chosen based on the results in [48].

During rapid solidification, solute supersaturation in the matrix can be illustrated by the extension of solute solid solubility due to high undercooling. Thus, there is no need for solutionizing so that samples can be directly aged after solidification, during which finely dispersed precipitates within the matrix are expected. Hence, aging of the as-collected IA samples was carried out following the second heat treatment approach, HT2, where the as-collected IA samples were heated to 300°C (Step 1), held for 20 h (Step 2) and then water quenched to room temperature (Step 3).

3. Results and Discussions

3.1. Effect of Sc on as-solidified Al-4.5 wt% Cu

3.1.1. Microstructure

a) ND analysis

XRD analysis of the Al-4.5 wt% Cu-xSc samples (x= 0.1, 0.2 and 0.4 wt%) showed the presence of only two phases, namely α-Al and θ-Al_2Cu, for both Sc-containing and Sc-free samples [50]. However, because of the higher penetration depth of neutrons relative to x-rays, ND analysis was carried out on the as-atomized Al-4.5 wt% Cu-xSc (x = 0.0, 0.1, 0.2 and 0.4 wt%) samples, so that the entire volume of the samples could be analyzed.

[Figure 1 near here]

Typical ND patterns of Al-4.5wt% Cu-xSc (x= 0.1, 0.2 and 0.4 wt %) droplets of average size 275 *μm*, atomized in Ar, are shown in Figure 3a. As summarized in Table 1, for all the investigated samples, the diffraction patterns, independent of the Sc content, showed evidence of two phases: α-Al and θ-Al_2Cu. These results suggest that the volume fraction of Sc-bearing precipitates, if there are any, must be too low to be detected by ND. The lower detection limit of ND is a function of the peak to background ratio, so each sample was scanned twice (3 hours for each scan) and the

7

patterns were summed to obtain 6 hours of data. In addition, an experiment with an empty crucible was carried out to enable the subtraction of miscellaneous peaks.

[Table 1 near here]

Indeed, due to the supersaturation of the solute elements in the primary α-Al matrix during rapid solidification, the pro-eutectic liquid would be depleted of Cu and Sc, preventing formation of secondary Sc-bearing precipitates and leading to less than the equilibrium amount of Cu-bearing precipitates in the final microstructure. Moreover, the incorporation of solute changes the effective lattice spacing of the α-Al matrix phase. Lubarda [51] and Axon and Hume-Rothery [52] have shown that the effective lattice spacing of α-Al decreases as Cu concentration increases. In addition, Royset reported that the lattice parameter of the Al matrix increases linearly with increasing Sc content in solid solution, but the solid solubility of Cu in Al decreases with increasing Sc content while the solubility of Sc in Al is not influenced by the Cu content [53]. Because of the variation of Cu and Sc content in the α-Al matrix, significant asymmetry of the α-Al peaks was observed (Figure 3b). According to the equilibrium phase diagrams shown in Figure 1, Cu is soluble in Al to a maximum of ~5.6 wt% at 550°C while the maximum solubility of Sc is ~0.38 wt% at 660°C. The maximum solubility of each element is expected to increase by undercooling the melt below T_E (the equilibrium nucleation temperature of the eutectic as indicated in Figure 1), so that more solute is trapped in the α-Al phase leading to a modification of its effective lattice spacing.

Rietveld refinement analysis was carried out to fit the diffraction peaks of all the investigated samples and the volume fraction of each phase was determined. As shown in Figure 4, in all cases, the fraction of θ-Al_2Cu is relatively lower than the Gulliver-Scheil (GS) model prediction. Within the error bars of the measurements, Sc-containing samples yielded approximately the same fraction of θ-Al_2Cu phase as the Sc-free samples, suggesting that the fraction of eutectic is more influenced by rapid solidification than by the level of micro-addition of Sc. The solidification cooling rate, $\dot{T}$, was obtained using Wiskel's heat transfer model of an atomized droplet [32], [33].

[Figure 4 near here]

8

As mentioned earlier, due to the variation in the Cu and Sc content in the α-Al matrix, significant asymmetry of the α-Al peaks was observed. The symmetry was taken into account, during Rietveld refinement, by considering up to four α-Al phases with slightly different lattice spacings. An average value of lattice spacing could then be calculated by taking a weighted average of the measured lattice spacings for the four α-Al phases based on their fraction.

Figure 5 shows the variation, with eutectic nucleation undercooling, of the estimated average lattice spacing of α-Al (Figure 5a) and the corresponding average amount of dissolved Cu (Figure 5b) for all investigated samples. The eutectic nucleation undercooling for each sample was determined by extending the solidus and liquidus lines of the Al-Cu binary phase diagram and the Al-4.5 wt% Cu-xSc (x= 0.1 wt%, 0.2 wt% and 0.4 wt%) pseudo-binary phase diagrams using Thermo-Calc [10]. A detailed description of the procedure is given in [34].

[Figure 5 near here]

In all cases, Figure 5a shows that the average lattice spacing is significantly smaller than 4.0496 Å, the lattice spacing of pure Al [51]. This result is expected, as Cu and Sc are incorporated in the α-Al phase during rapid solidification. It is worth noting that, the atomic radius of Cu (r(Cu) = 0.1278 nm)) is about 10.8% smaller than that of Al (r(Al) = 0.1432 nm)), while Sc atoms (r(Sc) =0.162 nm)) are about 11.6% larger than Al atoms [52][54]. Thus, the combined effect of dissolved Cu (decreases the lattice parameter of the α-Al solid solution) and Sc (increases the lattice parameter of the α-Al solid solution) leads to little or no distortion of the α-Al lattice, so that any solution strengthening will be negligible. As shown in Figure 5b, the average weight fraction of dissolved Cu in α-Al after solidification is higher than the equilibrium maximum solubility for Al-Cu alloys (~5.6 wt%) and this amount increases with increasing undercooling. This explains the relatively small average lattice spacing of α-Al. Although a numerical value could not be obtained (no Sc-bearing secondary phase was observed), a higher than equilibrium maximum solubility of Sc in the α-Al phase is expected after rapid solidification.

a) SEM analysis

Figure 6a and 6b show SEM backscattered electron (BSE) micrographs representing, respectively, typical surface and cross section microstructures of the investigated samples. It is clear that the

microstructure is cellular in nature, indicating that the IA droplets experienced rapid solidification characterized by a high growth velocity as described by Kurz and Fisher [55]. The image in Figure 6b shows evidence of two phases characterized by different grey levels. The Al-rich matrix (α-phase) is dark, while the eutectic structure, consisting of Cu-rich θ-Al_2Cu + α, appears white.

[Figure 6 near here]

b) EPMA analysis

Figure 7 shows x-ray maps for Al, Cu and Sc from an as-collected Al-4.5 wt% Cu-0.4 wt% Sc IA droplet with an average diameter of 230 µm. Figure 7b shows that the primary α-Al phase (indicated in Figure 7a) is Al-rich, while Cu and Sc are mostly located at the α-Al cell boundaries (Figure 7c and 7d). However, there is evidence of Cu (and Sc) dissolved within the primary α-Al phase, trapped in solution during rapid solidification, which confirms the ND results.

[Figure 7 near here]

c) TEM analysis

TEM analysis of the α-Al matrix and the inter-cellular regions of an Al-4.5 wt% Cu-0.4 wt% Sc IA droplet in He (230 µm average size, $\dot{T}=10^4\,Ks^{-1}$) is shown in Figure 8. A bright field (BF) image of the microstructure is shown in Figure 8a where the regions marked 1 and 2 indicate, respectively, the α-Al matrix and the inter-cellular region. A selected area diffraction (SAD) pattern of the matrix phase (region 1) has been indexed to α-Al (Figure 8b), while region 2 has been indexed to θ-Al_2Cu. No other phases (Al_3Sc or W-phase) were detected; however, it is worth noting that Sc peaks can be seen in the EDX spectra for both the matrix and the inter-cellular regions, due to dissolution of Sc in the α-Al and θ-Al_2Cu phases. There is more Sc dissolved in the θ-Al_2Cu precipitate than in the matrix phase.

[Figure 8 near here]

3.1.2. Microstructural length scale and mechanical properties

a) Cell spacing variation

In order to determine the effect of Sc on the dimensions of the as-solidified microstructure, the cell lengths (λ) were measured for a wide range of solidification cooling rates, $\dot{T}$. Figure 9 shows that λ varies from 5 μm to 100 μm within the limits of the investigated $\dot{T}$ for Al-4.5 wt Cu-xSc (x= 0.0, 0.1, 0.2 and 0.4 wt%). The plotted data include, in addition to the IA results, λ values measured on samples generated by electro-magnetic levitation (EML) [56] and differential scanning calorimetry (DSC) [9], which account for the medium range of $\dot{T}$ (4 Ks^{-1} to 15 Ks^{-1}) and lower range of $\dot{T}$ (0.01 Ks^{-1} to 0.8 Ks^{-1}), respectively, relative to IA (10^2 Ks^{-1} to 10^4 Ks^{-1}). Cell length measurements for IA samples published by Wiskel et al [33] are also included. Figure 9 shows that, independent of the Sc content, λ versus $\dot{T}$ can be fit to Equation 1. High cooling rates, which lead to large undercooling, during rapid solidification are the dominant factor affecting cell size, relative to the level of Sc, so that the effect of Sc is negligible.

$$\lambda = 86\dot{T}^{-0.35} \qquad (1)$$

Equation 1 follows the general reported expression shown in Equation 2.

$$\lambda = A\dot{T}^{-n} \qquad (2)$$

where *A is* a constant expressed in μm-(Ks^{-1})^n and *n* is a dimensionless constant. The values for *n* and *A* reported here fall within the range of values (0.29-0.41 μm-(Ks^{-1})^n and 43.4-87.2, respectively) reported in the literature for Al-Cu alloys with 4 to 5 wt% Cu solidified at cooling rates varying from 0.01 Ks^{-1} to 2×10^4 Ks^{-1} by various solidification techniques [57], [58].

[Figure 9 near here]

b) Vickers Microhardness

Vickers microhardness variation with $\dot{T}$ is plotted in Figure 10. The results include, IA samples, as well as EML [56] and DSC [9] samples. In all cases, the hardness (HV) is around 60 HV. These

results show that the addition of Sc up to 0.4 wt% to a hypoeutectic Al-4.5wt% Cu alloy does not produce a stronger material upon solidification, independent of the cooling rate applied. This suggests that the undercooling induced dissolution of Cu and Sc in the matrix does not contribute to the improvement in the mechanical properties of rapidly solidified samples. This result was expected since the α-Al lattice remains undistorted due to the combined effect of dissolved Cu (decreases the lattice parameter of the α-Al solid solution) and Sc (increases the lattice parameter of the α-Al solid solution). Indeed, the degree of strengthening imparted by the dissolution of an alloying element in the matrix depends on the resulting distortion of the crystal lattice, which impedes the progress of dislocations leading to higher strength. As mentioned earlier (ND analysis section), the α-Al matrix is influenced by both dissolved Cu and Sc; the former decreases the lattice parameter while the latter increases the lattice parameter. Consequently, the combined effect leads to a very little distortion of the α-Al lattice and, as such, minimal effect on the microhardness due to solute strengthening is observed. However, locally, Sc will produce a compressive strain field, while Cu will produce a tensile strain field. Even though there is little change in the lattice parameter because of the competing effects, there will be local strain fields which should affect the strengthening, i.e., interact with the strain fields of dislocations and block their motion. Hence the variation of hardness around 60 HV.

[Figure 10 near here]

3.1. Effect of Sc on heat treated Al-4.5 wt% Cu

3.1.1. Effect of Sc on precipitation hardening

a) EPMA results

Figure 11 shows x-ray maps for Al, Cu and Sc from a section of an HT2 heat treated Al-4.5 wt% Cu-0.4 wt% Sc sample fabricated by IA in He (average size of 230 µm, $\dot{T}=10^4\ Ks^{-1}$). A high magnification SEM image of the section (in BSE mode) is shown in Figure 11a. The microstructure consists of the Al-rich matrix (α-phase, dark) and the Cu-rich eutectic regions (white), with no evidence of fine precipitates within the Al-rich matrix. Elemental maps for Al, Cu and Sc are shown in Figure 11b to 11d; the elemental distributions are similar to the as-collected IA sample

12

(Figure 7). The microstructure of the aged sample shows a primary phase consisting mostly of Al with some dissolved Cu and Sc, which are concentrated in the inter-cellular regions.

[Figure 11 near here]

Kinetic limitations during precipitate growth, induced by limited diffusivity of Sc and Cu in α-Al, may have resulted in small Sc- or Cu-rich precipitates that are not detectable at the resolution of the SEM. The root-mean-square (RMS) diffusion distance of Sc and Cu in Al is $\sqrt{4Dt}$, where D is the diffusivity of Sc or Cu in Al and is exponentially dependent on temperature, as illustrated in Equation 3 [59] and Equation 4 [60], where t is the aging time.

$$D_{Sc}(m^2/s) = (2.65) \times 10^{-4} \, (m^2/s) \, exp\left(-\frac{(168)(kJ/mol)}{RT}\right) \qquad (3)$$

$$D_{Cu}(m^2/s) = (1.0) \times 10^{-5} \, (m^2/s) \, exp\left(-\frac{(127.6)(kJ/mol)}{RT}\right) \qquad (4)$$

R is the gas constant (0.0083144 kJ/mol-K) and T is the absolute temperature (in K).

The RMS diffusion distance for t = 20 h and T= 300°C (573 K) is 192 nm for Sc. This distance is about 25 times smaller than the cell length of the corresponding droplet microstructure. Consequently, any diffusion of Sc in the α-Al will be constrained within the matrix cell so that any Al₃Sc precipitates within the matrix are likely to be small and difficult to detect by SEM. Similarly, any Sc in the inter-cellular regions is likely to precipitate within these regions. For Cu, the RMS diffusion distance for t = 20 h and T= 300°C (573 K) is 2.6 µm, which is about half the average cell length of the corresponding droplet microstructure. Therefore, equilibrium θ-Al₂Cu or the transition phases (θ"-Al₂Cu and θ'-Al₂Cu) can be expected to nucleate within the matrix through the diffusion of Cu from the cell-boundaries and these precipitates should be larger than the Al₃Sc precipitates. It has been reported that Sc segregation promotes the precipitation of θ'-Al₂Cu/θ-Al₂Cu during aging treatment [61].   TEM is required to detect and identify these precipitates.

b) TEM results

TEM analysis was carried out on the HT2 heat treated Al-4.5 wt% Cu-0.4 wt% Sc droplet fabricated by IA in He (average size of 230 µm, $\dot{T}=10^4\,Ks^{-1}$). Figure 12 shows a STEM annular dark field (ADF) micrograph (Figure 12a) where there is evidence of relatively large precipitates (30-300 nm) and much smaller precipitates (~10 nm) within the α-Al matrix. An X-ray line scan across the smaller precipitates shown in Figure 12b reveals that these precipitates contain Al and Sc but no Cu (an expanded EDX line scan for Sc is included in Figure 12b to clearly show the evidence of Sc). Based on this line scan, the Sc-bearing precipitates are proposed to be Al_3Sc. The larger precipitates, meanwhile, consist of Al and Cu, with some Sc, as indicated by the corresponding EDX spectrum in Figure 12c. The SAD pattern (inset of Figure 12c) from the larger precipitate indicated in Figure 12a is indexed to θ-$CuAl_2$ with a [1$\underline{4}$2] zone axis. The composition of the precipitate, consisting of Sc, Cu and Al, suggests that its precipitation may have heterogeneously been promoted by Sc as reported in [61]. The other smaller precipitates shown in Figure 12a are also θ-$CuAl_2$.

[Figure 12 near here]

3.1.2. Mechanical properties

The variation in microhardness with Sc addition for the four investigated thermal histories, i.e., as-solidified by DSC, as-collected after IA and heat treated under HT1 and HT2 conditions, is shown in Figure 13.

[Figure 13 near here]

The microhardness increases slightly with increasing Sc level for the as-collected IA samples, as well as for the as-solidified by DSC samples (results taken from [9]). This indicates that as more Sc is present in the initial liquid, the matrix will become more supersaturated upon solidification. The samples subjected to HT1 condition show an increase in microhardness relative to the as-solidified by DSC and as-collected IA samples, for Sc levels ≤ 0.1 wt%. Indeed, with this level of

Sc addition, precipitation of θ'-Al$_2$Cu/θ-Al$_2$Cu is more favorable upon aging, as there is more supersaturated Cu in the matrix, since Sc somewhat reduces the solid solubility of Cu in Al [53].

For Sc levels > 0.1w%, the microhardness decreases for the HT1 condition and is similar to that for the as-solidified DSC and as-collected IA samples. This low hardness can be attributed to the partial consumption of the Sc and Cu atoms for the formation of white contrast precipitates (Figure 14a and 14b), which are identified as the ternary W-phase in [50] . The formation of the ternary W-phase, which occurs during solutionizing (Step 2 of HT1), can be explained by one of two hypotheses: (i) W-phase formation may have been induced by diffusion of Sc from either primary or the eutectic α-Al. (ii) W-phase formation may be the result of thermally activated transformation of the Sc-containing θ-Al$_2$Cu phase at 535°C. Using the RMS diffusion distance of Sc in Al, it can be shown that Sc can diffuse through a distance of ~30 µm during solutionizing at 535°C for 18.5 h. This distance is about 6 times larger than the average cell length of the corresponding droplet microstructure. The consequence of W-phase formation is the minimization of the amount of Cu and Sc elements in the matrix and the subsequent precipitation of any strengthening Cu-/Sc-rich phase upon aging.

[Figure 14 near here]

For samples subjected to HT2, Figure 14 shows that the microhardness gradually increases with increasing Sc level, due to rapid solidification induced more Sc dissolution in the matrix (and no W-phase formation), resulting in the formation of more Sc-bearing precipitates upon aging, which cause lattice distortions that impede the movement of dislocations.

At the highest level of Sc (0.4 wt%), the microhardness reaches 120 HV, which is much higher than all the other investigated samples. This value, converted into yield stress, is about 250 MPA [62] which represents an increase of about 100 MPa in yield stress from the 90 HV obtained for the Al-4.5 wt% Cu sample after the classical heat treatment procedure (HT1). This result suggests that by aging a rapid solidified hypoeutectic Al-Cu-Sc alloy, some heat treatment processing steps (solutionizing and quenching) may be eliminated while still generating superior mechanical properties. It is worth noting that the degree of strengthening is highly dependent on the aging process, the average size, the volume fraction and the size distribution of the precipitates. However, investigation of these parameters is out of the scope of the present contribution.

3.   Conclusions

Rapid solidification of hypoeutectic Al-Cu with micro-additions of Sc has been studied by a combination of several complementary analytical tools. The following conclusions can be drawn from this study.

- No Sc-bearing precipitate was observed in the microstructures of the as-atomised powder.
- Micro-additions of Sc (up to 0.4 wt%) in Al-4.5 wt% Cu alloys did not produce grain refinement of the rapid solidified microstructure.
- Undercooling induced solubility extension of Cu and Sc and led to a reduction of the α-Al lattice size.
- The combined effect of dissolved Cu (decreases the lattice parameter of the α-Al solid solution) and Sc (increases the lattice parameter of the α-Al solid solution) led to little or no distortion of the α-Al lattice, so that solution strengthening was negligible.
- Nano-precipitates of Sc were observed in the matrix following the aging treatment. These precipitates were deemed to be responsible for the dramatic increase in hardness recorded.
- A microhardness value of 120 HV, which is equivalent to a yield stress of ~250 MPa, was obtained after direct aging of as-atomised Al-4.5 wt% Cu-0.4 wt% Sc IA samples (HT2 protocol). This value represents an increase of about 100 MPa in yield stress compared with a solutionized, quenched and aged Al-4.5 wt% Cu sample (HT1 protocol).
- Direct aging of a rapidly solidified hypoeutectic Al-Cu-Sc alloy is a time and cost effective processing route. As such, Sc as a hypoeutectic alloy addition is beneficial, specifically for rapidly solidified Al alloys through processes such as strip casting, die-casting, atomization and additive manufacturing. Solutionizing and quenching steps may be eliminated as part of the age hardening process and replaced with just an aging treatment following rapid solidification.

References

[1] F. Casarotto, A. J. Franke, and R. Franke, *Advanced Materials in Automotive Engineering*, 2012, 109–149.

[2]   J. C. Benedyk, *Materials, Design and Manufacturing for Lightweight Vehicles*, 2010, 79–113.

[3]   M. Garat and G.Laslaz, *Am. Foundry Soc.*, 2007, 1–8.

[4]   W.S. Miller, L. Zhuang, J. Bottema *et al.*, *Mater. Sci. Eng. A*, 2000, 280:1, 37–49.

[5]   R.Molina, P.Amalberto, M.Rosso, *Metall. Sci. Technol.*, 2011, 29:2, 5–13.

[6]   E. A. Starke and H. M. M. A. Rashed, *Reference Module in Materials Science and Materials Engineering*, 2017, 10.1016/B978-0-12-803581-8.09210-9

[7]   D. Emadi, A. K. P. Rao, and M. Mahfoud, *Mater. Sci. Eng. A*,2010, 527: 23, 6123–6132.

[8]   J. Royset, *Metall. Sci. andTechnology*, 2007, 25:2, 11–21.

[9]   A-A. Bogno, J. Valloton, H. Henein, D.G. Ivey, A.J. Locock, and M. Gallerneault, *Can. Metall. Q.*, 2017, 57:2, 148-159.

[10]   "Thermo-Calc Database, TTAL7 Version1.1." 2008.

[11]   J. O. Andersson, T. Helander, L. Höglund, P. Shi, and B. Sundman, *Calphad Comput. Coupling Phase Diagrams Thermochem.*, 2002, 26:2, 273–312.

[12]   P. Duwez, R. H. Willens, and W. Klement, *Journal of Applied Physics*, 1960, 31:6 1136–1137.

[13]   W. KLEMENT, R. H. WILLENS, and P. DUWEZ, *Nature*, 1960, 187:4740, 869–870.

[14]   H. A. Davies and J. B. Hull, *Mater. Sci. Eng.*, 1976, 23:2–3, 193–198.

[15]   M. G. Scott, *J. Mater. Sci.*, 1975, 10:2, 269–273.

[16]   H. S. Chen and D. Turnbull, *J. Chem. Phys.*, 1968, 48:6, 2560–2565.

[17]   R. C. Budhani, T. C. Goel, and K. L. Chopra, *Bull. Mater. Sci.*, 1982, 4:5, 549–561.

[18]   K. Katayama, K. Nakamura, and T. Amano, *Kolloid-Zeitschrift Zeitschrift für Polym.*, 1968, 226: 2, 125–134.

[19]   P. Liu, B. X. Kang, X. G. Cao, J. L. Huang, and H. C. Gu, *J. Mater. Sci.*, 2000, 35:7, 1691–1694.

[20]   A.J. Yule and J.J. Dunkley, *Oxford: Oxford Series on Advanced Manufacturing,Clarendon Press*, 1994.

[21]   J.J.Dunkley, *Powder Metall. Int.*, 1978, 10:1, 38–41.

[22]   A. H. Lefebvre, *A-to-Z Guid. to Thermodyn. Heat Mass Transf. Fluids Eng.*, 2013, 1,1–7.

[23]   D. Yuan, "The novel Impulse Atomization Process," University of Alberta, 1997.

[24] D. Aderhold, and J.J. Dunkley, *Powder Metallurgy and Particulate Materials*, 2007,26–31.

[25] S. Lagutkin, L. Achelis, S. Sheikhaliev, V. Uhlenwinkel, and V. Srivastava, *Mater. Sci. Eng. A*, 2004, 383:1 SPEC. ISS.,1–6.

[26] K.P.Olsen, G. Sterzik,and H.Henein, *Int. J. Powder Metall. (Princeton, New Jersey)*, 2001, 37:1,55–64.

[27] H. Henein, *Mater. Sci. Eng. A*, 2002, 326:1, 92–100.

[28] R. P. Liu, D. M. Herlach, M. Vandyoussefi, and a. L. Greer, *Metall. Mater. Trans. A*, 2004, 35:2, 607–612.

[29] J.Yu, P.F. Paradis, T.Ishikawa, S.Yoda, S.Ozawa *et al.*, *Japanese J. Appl. Physics, Part 1 Regul. Pap. Short Notes Rev. Pap.*, 2002, 41:5 A, 2908–2911.

[30] J. Yu, N. Koshikawa, Y. Arai, S. Yoda, and H. Saitou, *J. Cryst. Growth*, 2001, 231:4, 568–576.

[31] R. P. Liu, T. Volkmann, and D. M. Herlach, *Acta Mater.*, 2001, 49:3, 439–444.

[32] J. B. Wiskel, H. Henein, and E. Maire, *Can. Metall. Q.*, 2002, 41:1, 97–110.

[33] J. B. Wiskel, K. Navel, H. Henein, and E. Maire, *Canadian Metallurgical Quarterly*, 2002, 41:2,193–204.

[34] A.-A. Bogno, P. D. Khatibi, H. Henein, and Ch.-A. Gandin, *Metall. Mater. Trans. A Phys. Metall. Mater. Sci.*, 2016, 47:9, 4606–461.

[35] W. Kasprzak, D. Sediako, M. Sahoo, M. Walker, and I. Swainson, *TMS Annual Meeting*, 2010, vol. 1.

[36] D. Sediako, W. Kasprzak, I. Swainson, and O. Garlea, *Supplemental Proceedings: Materials Fabrication, Properties, Characterization, and Modeling*, 2011, 2, 279–289.

[37] W. Kasprzak, D. Sediako, I. Swainson, M. Sahoo, and M. Walker, *Mater. Sci.*, 2009, 1, 568–571.

[38] W. Kasprzak, D. Sediako, M. Walker, M. Sahoo, and I. Swainson, *Metall. Mater. Trans. A Phys. Metall. Mater. Sci.*, 2011, 42:7, 1854–1862.

[39] D. G. Sediako and W. Kasprzak, *Metall. Mater. Trans. A Phys. Metall. Mater. Sci.*, 2015, 46: 9.

[40] D. Sediako and W. Kasprzak, *Light Metals 2012*, 2016, 355–364.

[41] D. Sediako and W. Kasprzak, *TMS Light Metals*, 2012.

[42] R. A. Young, *The Rietveld Method*. 1993.

[43] A. A. Coelho, *J. Appl. Crystallogr.*, 2018, 51:1, 210–218.

[44] J. L. H. Aaronson, M. Enomoto, *Mechanism of Diffusional Phase Transformations in Metals and Alloys*. 2010.

[45] A. K. Dahle, *Encyclopedia of Materials: Science and Technology*, 2001, 111–113.

[46] J.Røyset, N.Ryum, D.Bettella, A.Tocco, Z.Jia *et al.*, *Mater. Sci. Eng. A*, 2008, 483, 175–178.

[47] H. H. Jo and S. I. Fujikawa, *Mater. Sci. Eng. A*, 1993, 10.1016/0921-5093(93)90401-Y.

[48] Ch.-A. Gandin, Y. Bréchet, M. Rappaz, G. Canova, M. Ashby, and H. Shercliff, *Acta Mater.*, 2002, 50:5,901–927.

[49] S. Costa, H. Puga, J. Barbosa, and A. M. P. Pinto, *Mater. Des.*, 2012, 42, 347–352.

[50] A-A. Bogno, H. Henein, and M. Gallerneault, *Minerals, Metals and Materials Series*, 2018, Part F4, 1609–1616.

[51] V. A. Lubarda, "On the effective lattice parameter of binary alloys," *Mech. Mater.*, 2003, 35:1-2, 53-68.

[52] H. J. Axon and W. Hume-Rothery, *Proc. R. Soc. A Math. Phys. Eng. Sci.*, 1948, 10.1098/rspa.1948.0030.

[53] J. Røyset and N. Ryum, *Int. Mater. Rev.*, 2005, 50:1,19–44.

[54] N. N. Greenwood and A. Earnshaw, *Chemistry of the elements*. 1995, 1423-1449.

[55] W.Kurz and D.J.Fisher, *Fundamentals of Solidification*, 1998, 4th editio. CRC Press.

[56] A.-A. Bogno, J. Valloton, P. Natzke, S. Yin, D. M. Herlach, and H. Henein, *Materials Science and Technology Conference and Exhibition 2015, MS and T 2015*, 2.

[57] D. Eskin, Q. Du, D. Ruvalcaba, and L. Katgerman, *Mater. Sci. Eng. A*, 2005, 405:1–2,1–10.

[58] A. M. Mullis, L. Farrell, R. F. Cochrane, and N. J. Adkins, *Metall. Mater. Trans. B Process Metall. Mater. Process. Sci.*, 2013, 44:4, 992–999.

[59] A. K. Marcel, T.D. Wood, P.G.Sanders, S.L.Kampe, and D. Swenson , *Metall. Mater. Trans. A*, 2014, 54A:9, 3800–3805.

[60] Y.Du, Y.A.Chang, B.Huang, W.Gong, Z.Jin, *et al.*, *Mater. Sci. Eng. A*, 2003, 363:1, 140–151.

[61] C.Yang, P.Zhang, D.Shao, R.H.Wang, L.F. Cao, *et al.*, *Acta Mater.*, 2016. 119, 68-79.

[62] E. J. Pavlina and C. J. Van Tyne, *J. Mater. Eng. Perform.*, 2008, 17:6, 888–893.

Tables

Table 1: Summary of samples analyzed by ND

Alloy composition	Average droplet size (µm)	Solidification cooling rate (Ks^{-1})	Detected phases
Al-4.5 wt% Cu	230	10000	
	275	1500	
	463	800	
Al-4.5 wt% Cu-0.1 wt% Sc	275	1500	
	463	800	α-Al
Al-4.5 wt% Cu-0.2 wt% Sc	275	1500	θ-Al$_2$Cu
	463	800	
Al-4.5 wt% Cu-0.4 wt% Sc	230	10000	
	275	1500	
	463	800	
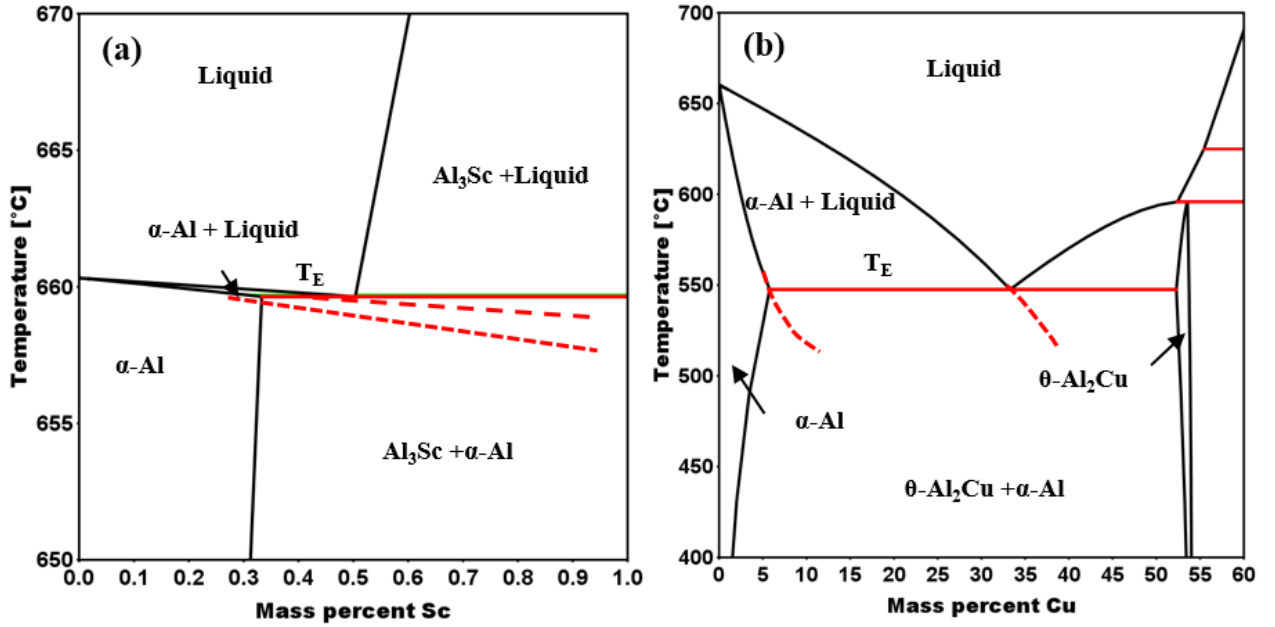
Figure 2: Al-rich corners of (a) Al-Sc and (b) Al-Cu binary phase diagrams. The dashed lines represent thermodynamic extensions of the solidus and liquidus lines obtained by Thermo-Calc, TTAL7 Version 1.1, 2008 [10, 11].
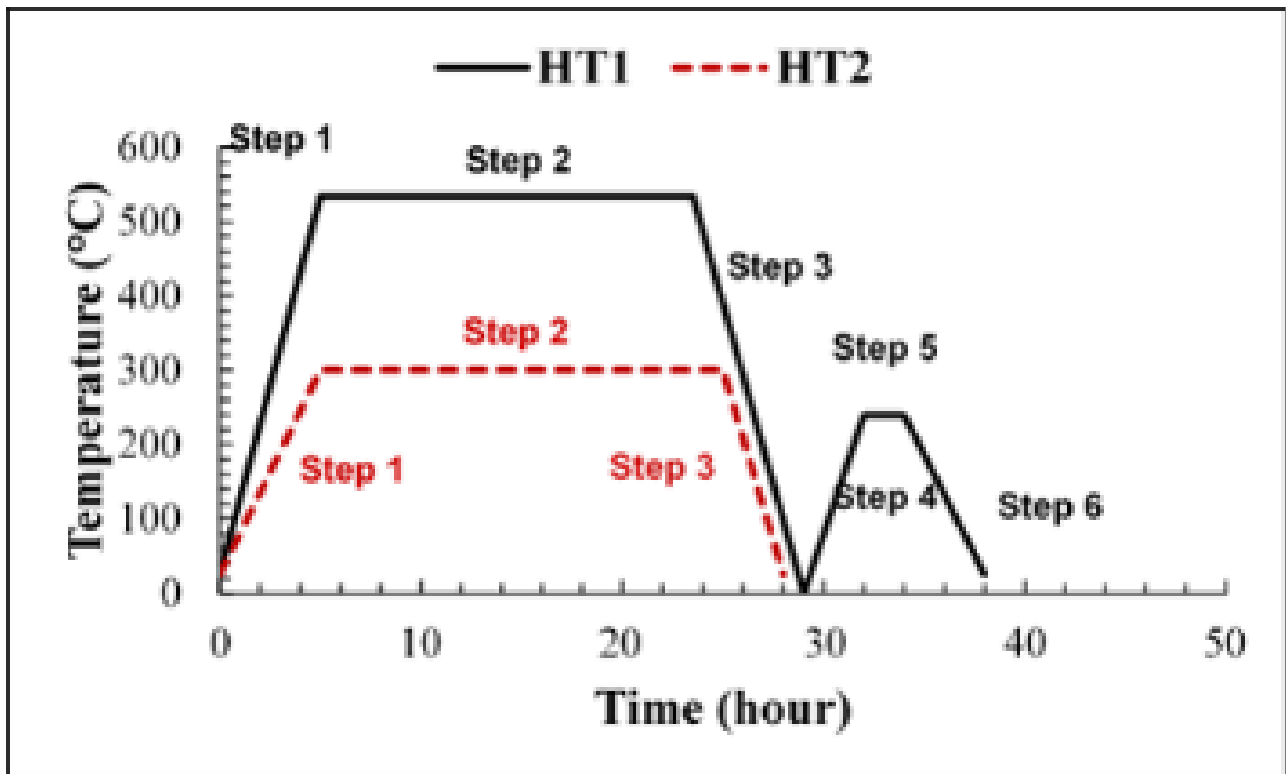
Figure 3: Schematic description of the two heat treatment approaches used in this study.
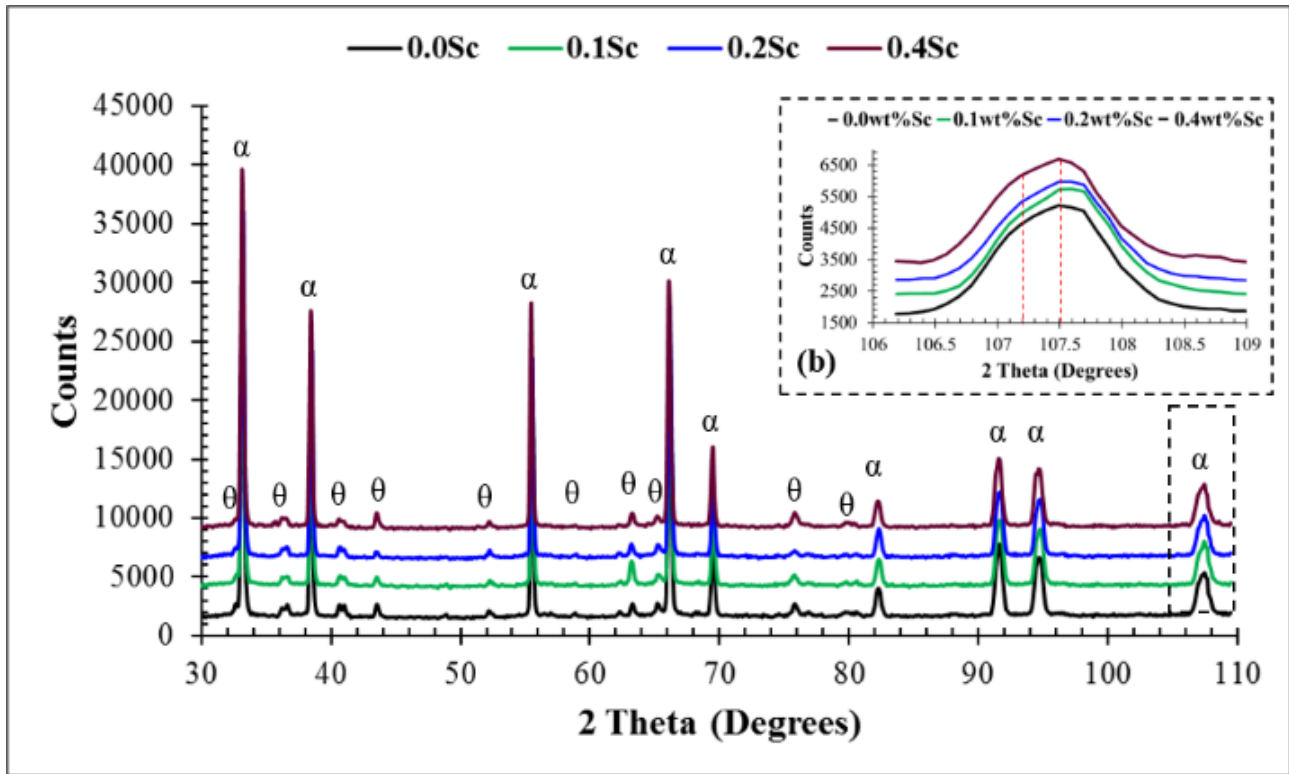
Figure 4: (a) ND patterns (neutron wavelength: 1.33 Å) for Al-4.5wt% Cu-xSc (x= 0.1, 0.2 and 0.4 wt %) droplets of average size 275 μm, atomized in Ar ($\dot{T}= 1.5 \times 10^3 \ Ks^{-1}$). (b) Magnified portion of the pattern, showing the asymmetric α-Al peak located around 107.5 degrees.
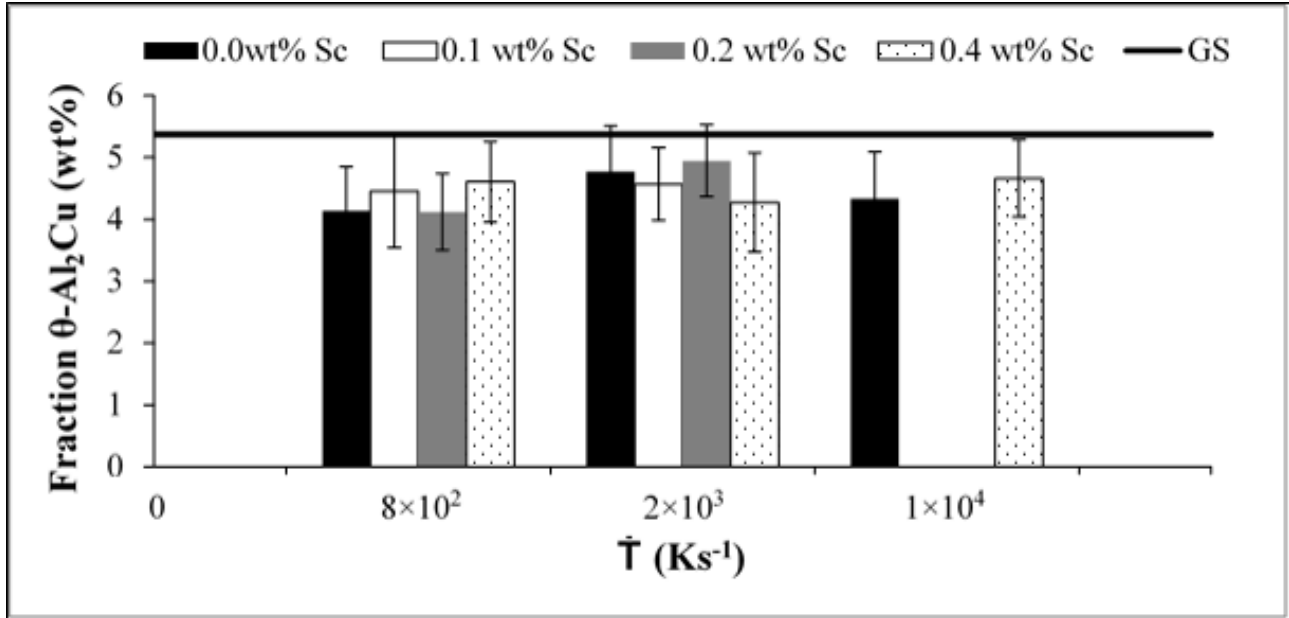
Figure 4: Variation of the estimated weight fraction of θ-Al₂Cu with solidification cooling rate Ṫ, for Al-4.5 wt% Cu-xSc (x= 0.0 wt%, 0.1 wt%, 0.2 wt% and 0.4 wt %).
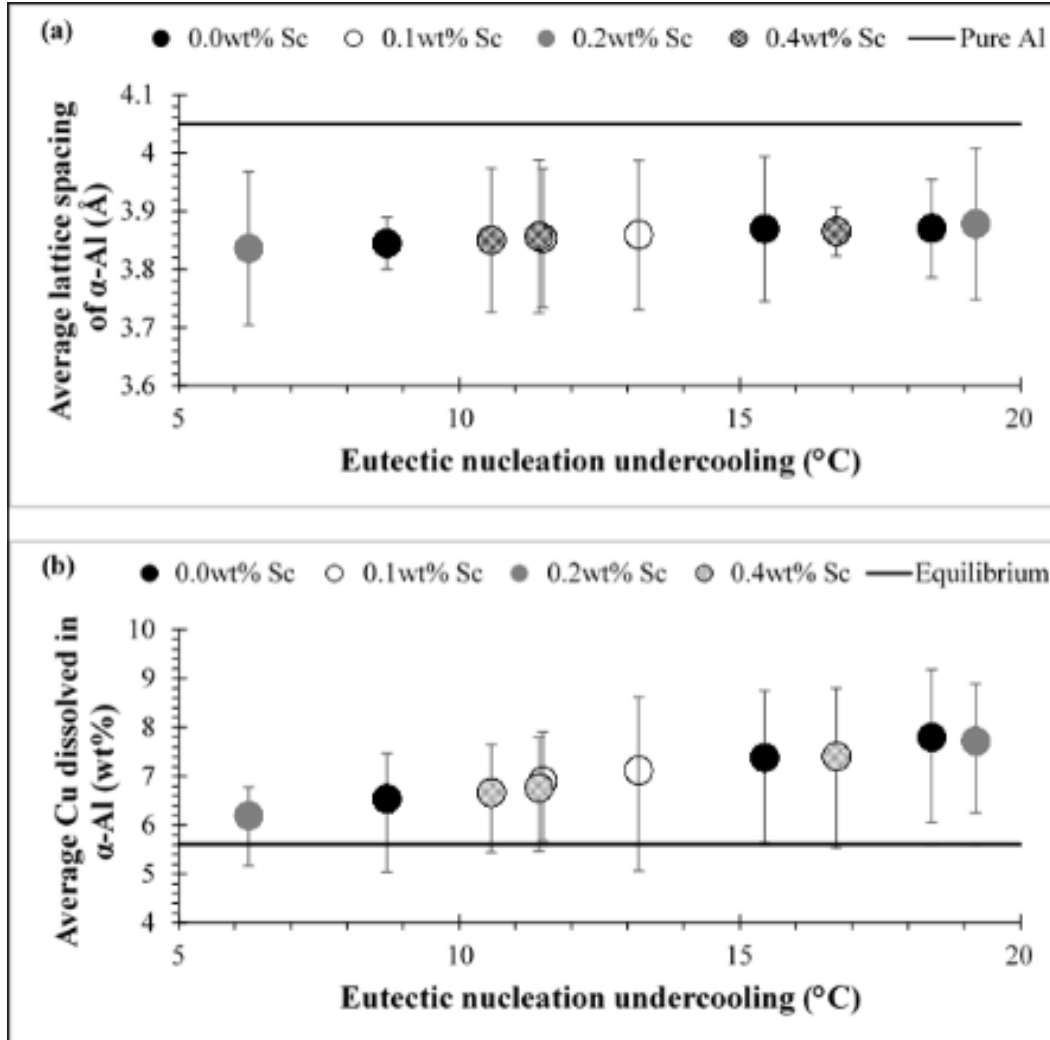
Figure 5: The effect of eutectic nucleation undercooling variation on (a) the lattice spacing of the primary α-Al phase and (b) the average amount of Cu dissolved in the primary α-Al phase, taken from the metastable phase diagram. The horizontal line in (a) represents the lattice parameter for pure α-Al, while the horizontal line in (b) represents the equilibrium solubility of Cu in α-Al.
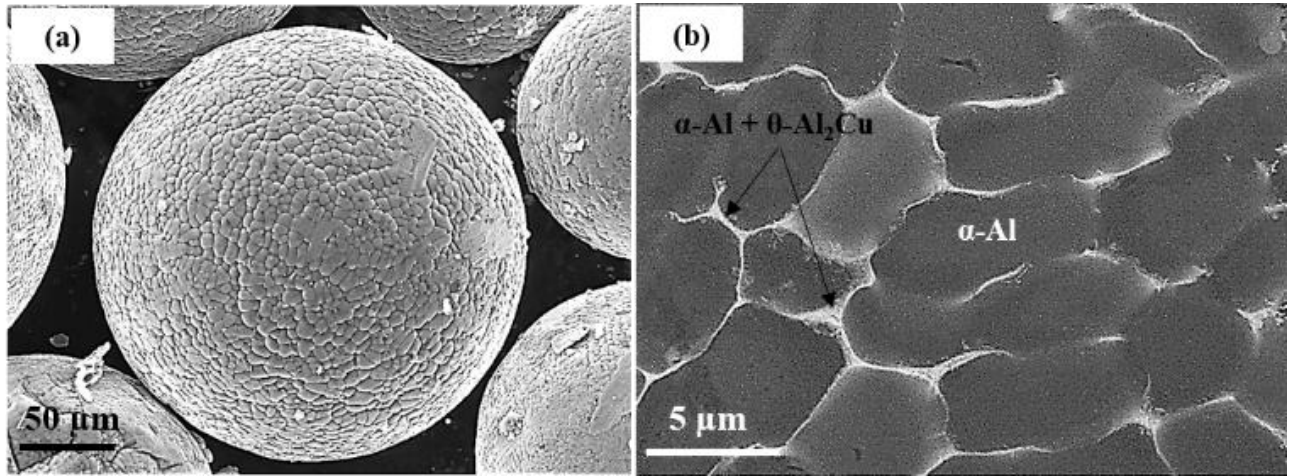
Figure 6: SEM BSE images of as-collected Al-4.5 wt% Cu-0.4 wt% Sc IA in He. (a) Droplet, 230 µm in diameter ($\dot{T}=10^4$ Ks^{-1}), covered with oxide and external defects. (b) Corresponding ground and polished section of a droplet from (a).
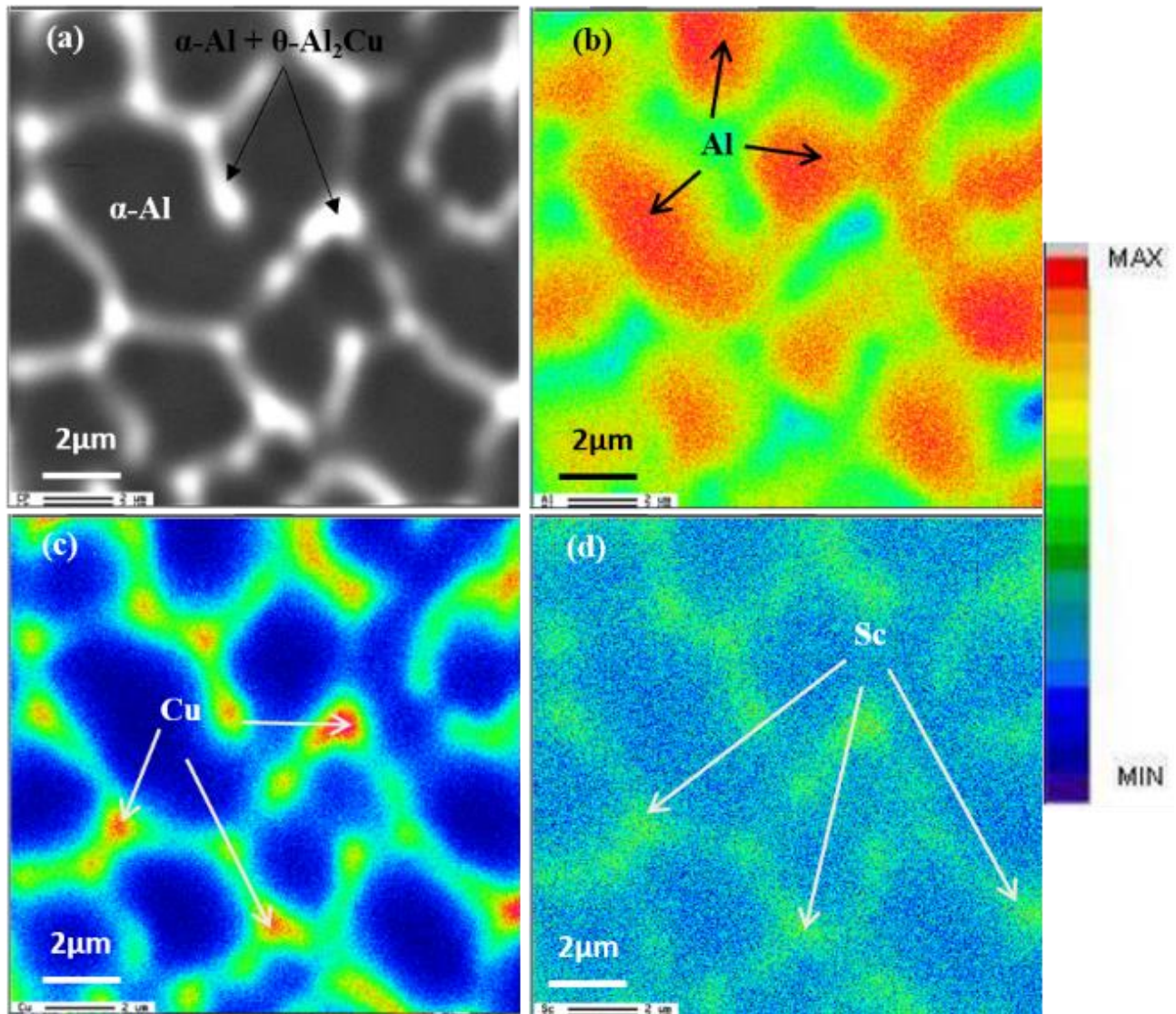
Figure 7: Electron microprobe elemental maps for an as-atomised Al-4.5 wt% Cu-0.4 wt% Sc IA droplet in He (average size of 230 μm and $\dot{T}=10^4$ Ks^{-1}). (a) SEM BSE image, (b) Al map, (c) Cu map and (d) Sc map.
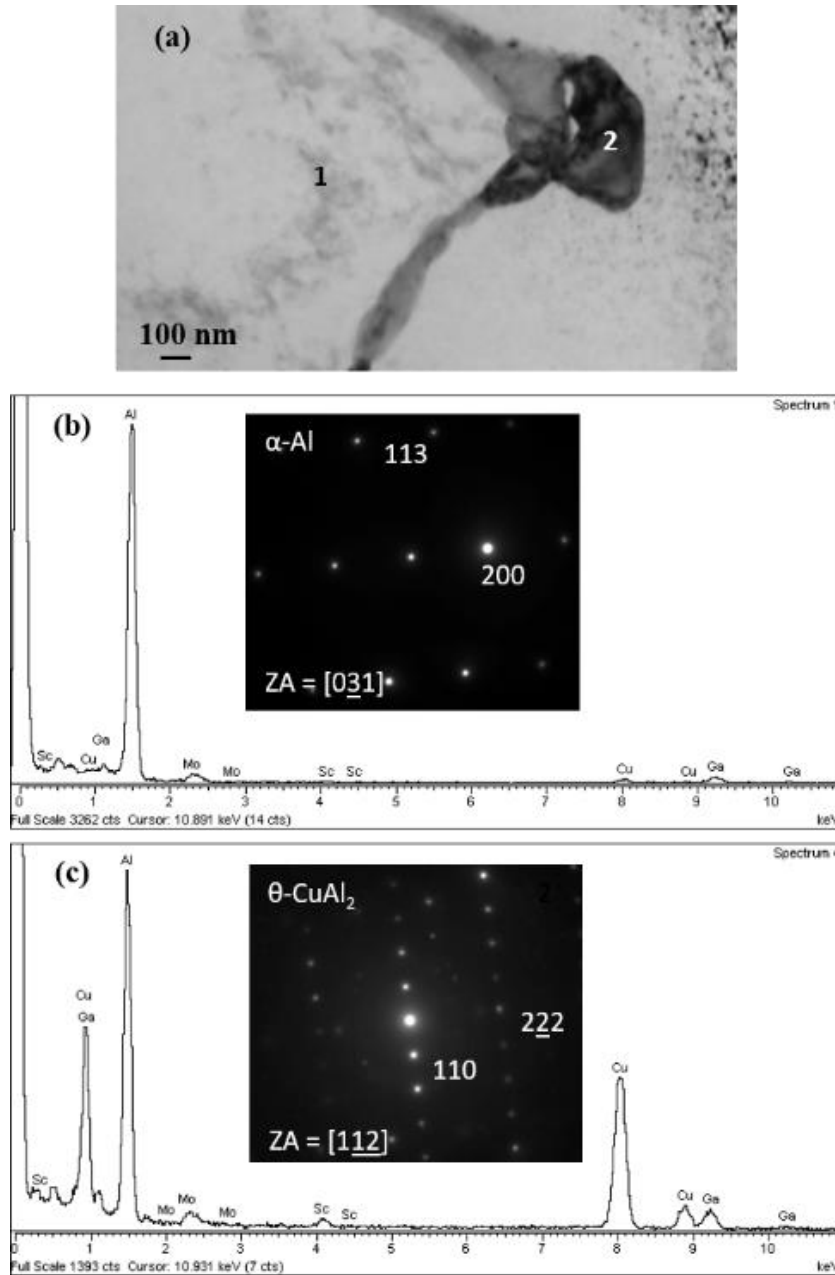
Figure 8: TEM analysis of an as-collected Al-4.5 wt% Cu-0.4 wt% Sc IA droplet in He (average size 230 µm, $\dot{T}=10^4$ Ks^{-1}). (a) TEM BF image, (b) diffraction pattern and EDX spectrum from region 1 in (a) and (c) SAD pattern and EDX spectrum from region 2 in (a). The Ga and Mo peaks in the EDX spectra are artifacts of FIB sample preparation.
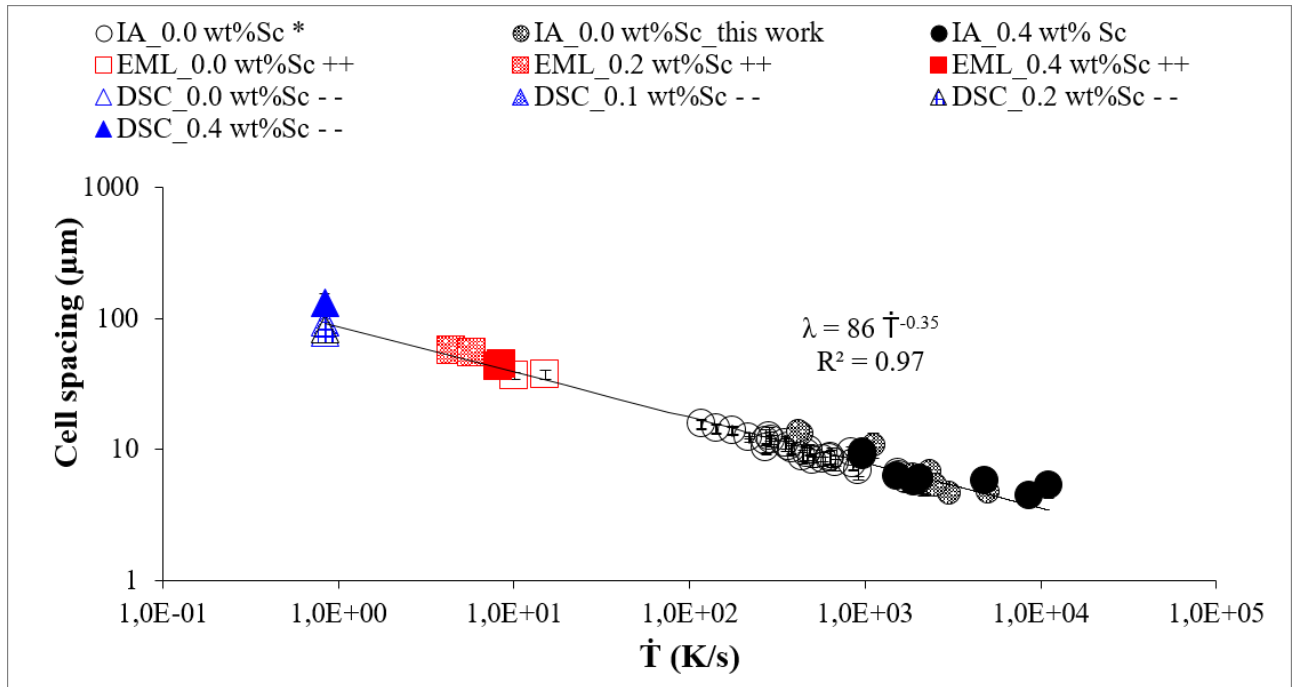
Figure 9: Variation of cell spacing with cooling rate for Al-4.5 wt% Cu – xSc (x= 0.0, 0.1, 0.2 and 0.4 wt %). * Data from Wiskel et al [33], ++ data from work in [56] and - - data from work in [9]
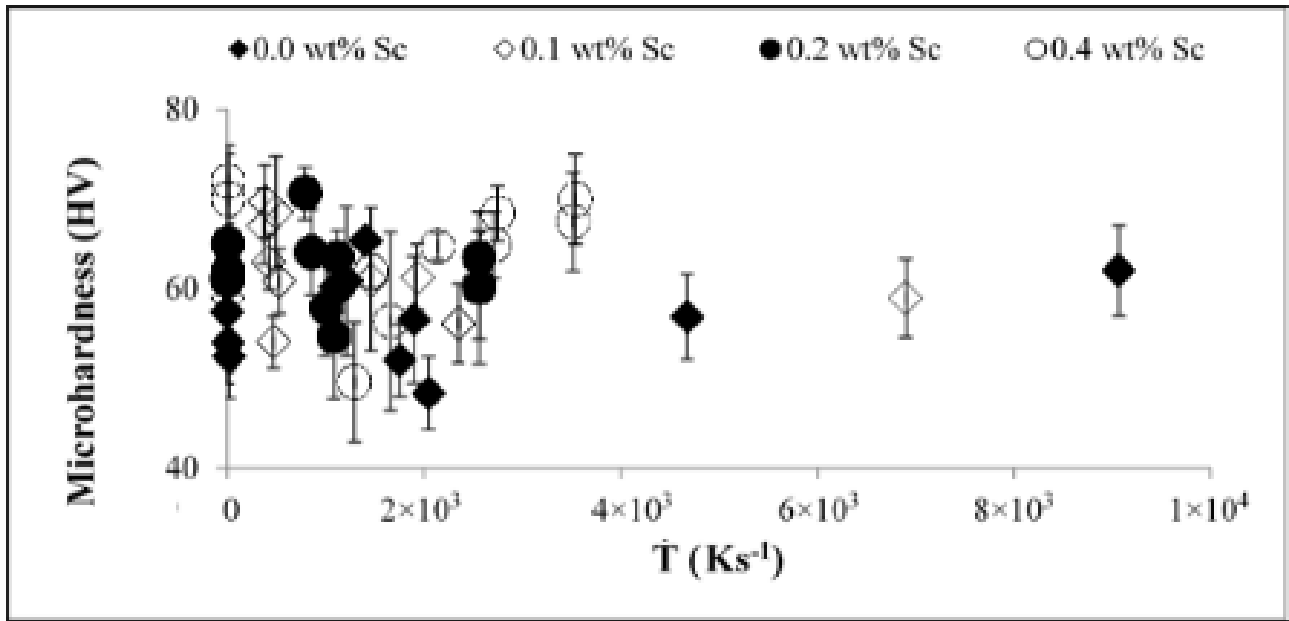
Figure 10: Variation of Vickers microhardness with cooling rate for Al-4.5 wt% Cu –xSc (x = 0.0 0.1, 0.2, and 0.4 wt%).
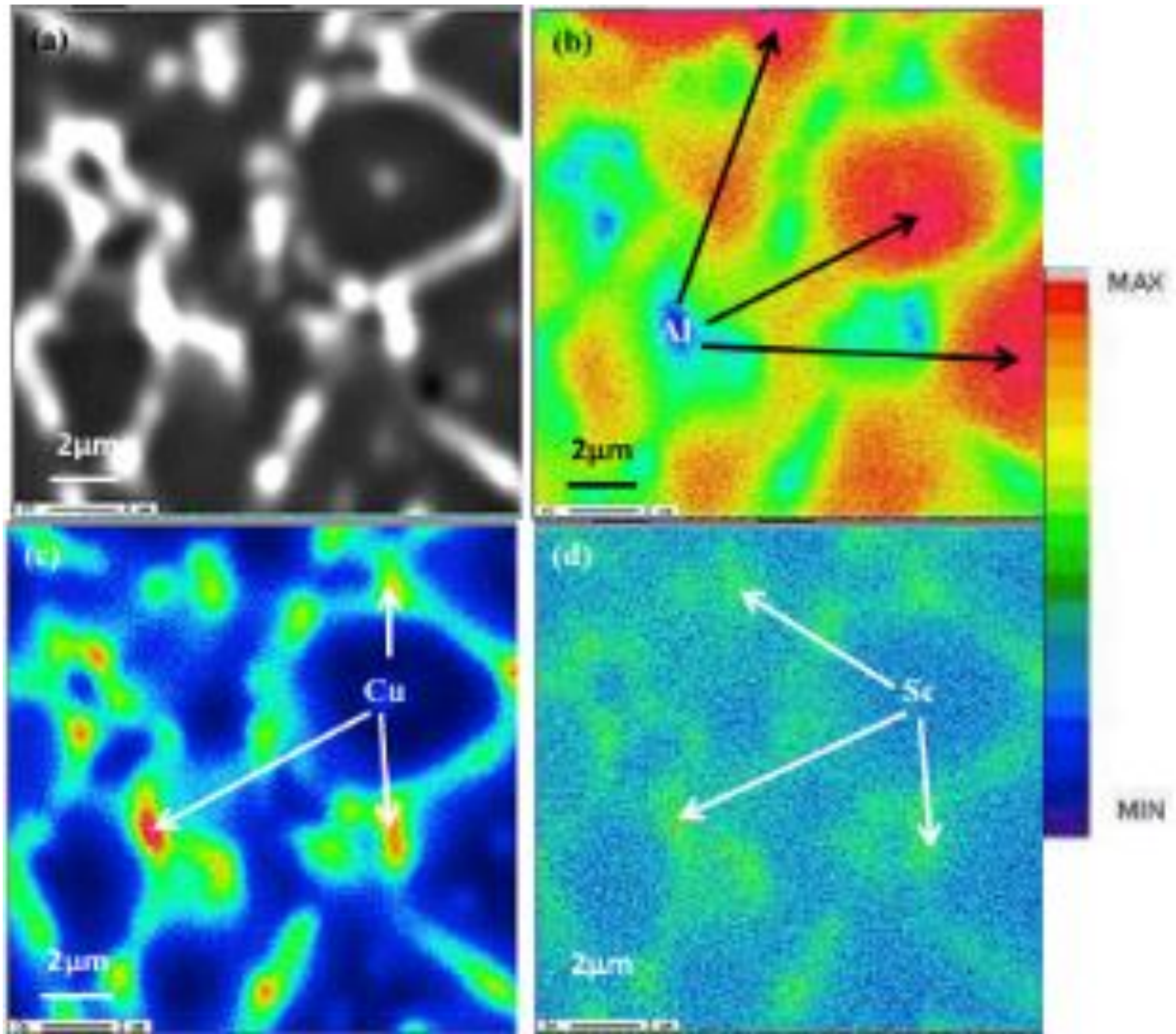
Figure 11: Electron microprobe element maps from a selected region of an Al-4.5 wt% Cu-0.4 wt% Sc droplet fabricated by IA in He (average size of 230 μm, $\dot{T}=10^4$ Ks^{-1}), which has undergone the HT2 heat treatment (aged at 300ºC for 20 h) . (a) SEM (BSE) image; (b) Al map, (c) Cu map and (d) Sc map.
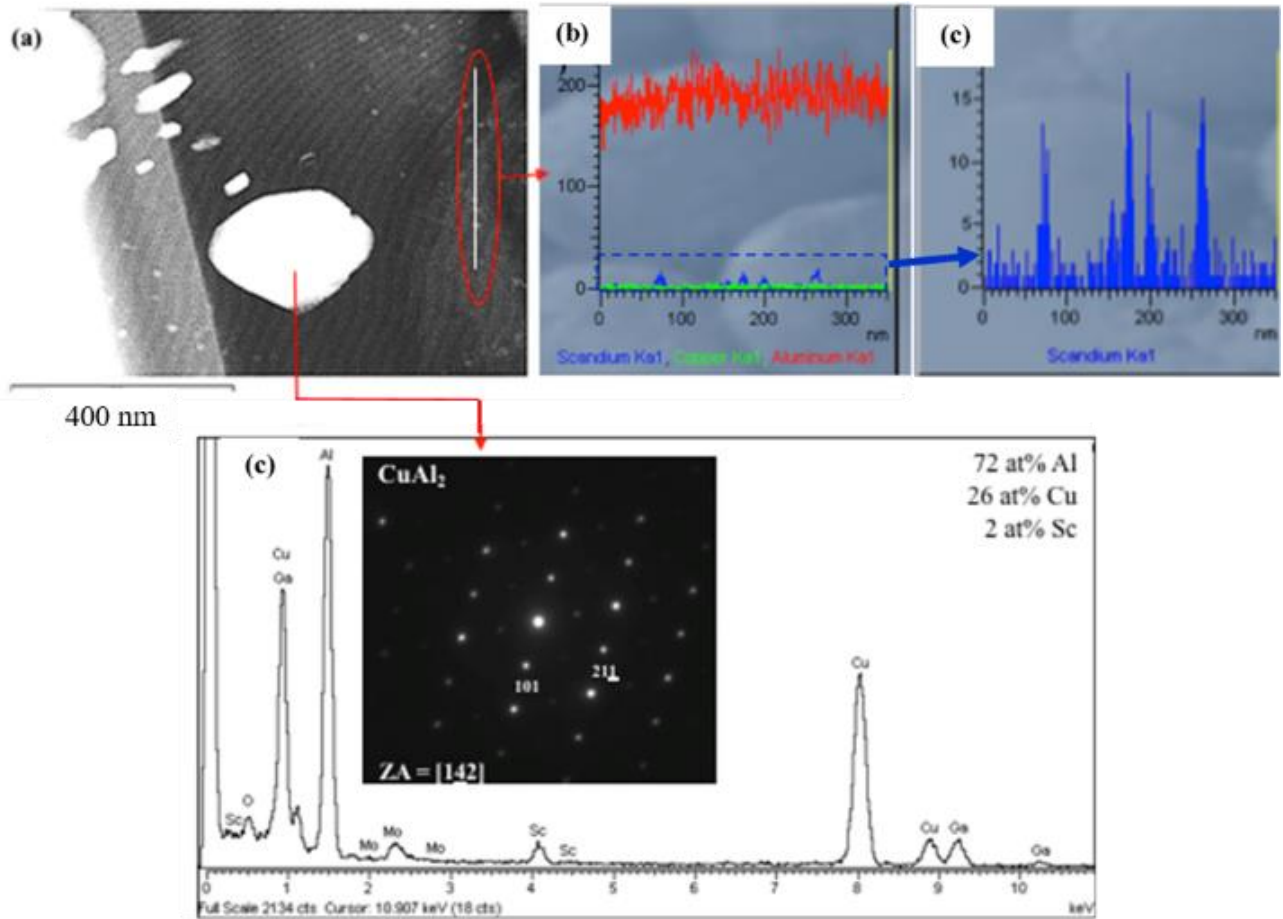
Figure 12:(a) STEM ADF image of Al-4.5 wt% Cu-0.4 wt% Sc sample fabricated by IA in He (average size of 230 μm, Ṫ=10⁴ Ks⁻¹) after aging at 300˚C for 20h. (b) X-ray line scan across the matrix and several fine precipitates from the region indicated in (a). (c) EDX spectrum and SAD diffraction pattern from the large θ-Al₂Cu precipitate in (a). The Ga and Mo peaks in the EDX spectrum are artifacts of FIB sample preparation.
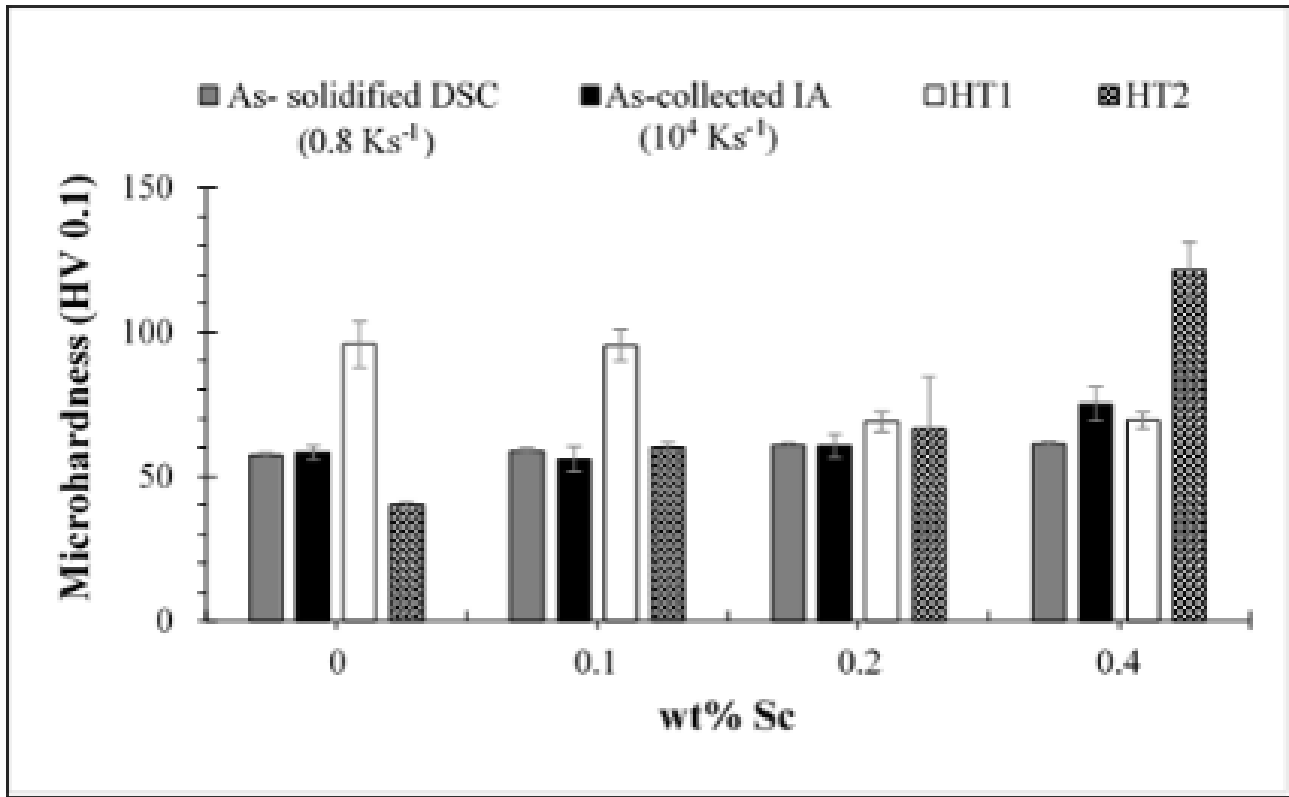
Figure 5: Variation in Vickers microhardness with Sc concentration in Al-4.5 wt% Cu - xSc (x= 0.0, 0.1, 0.2 and 0.4 wt %) samples with different thermal histories.
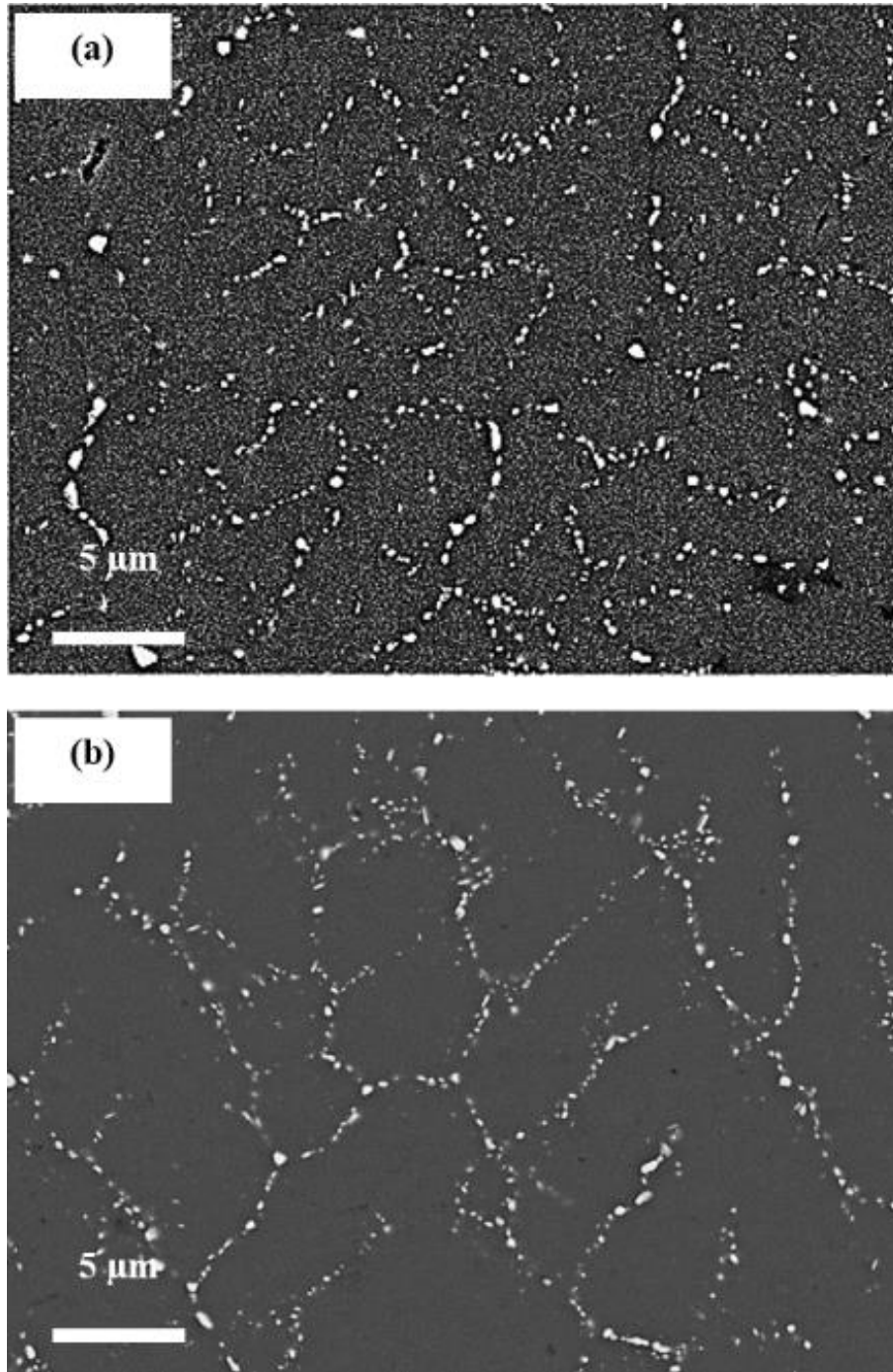
Figure 6: SEM BSE micrographs of samples subjected to HT1 treatment, after step 2. (a) Al-4.5 wt% Cu-0.4 wt% Sc, (b) Al-4.5 wt% Cu-0.2 wt% Sc. Average particle size is 230 µm; cooling gas is He.